AGU PUBLICATIONS

Earth's Future

RESEARCH ARTICLE
10.1002/2015EF000350

Terrestrial water flux responses to global warming in tropical rainforest areas

Chia-Wei Lan[1], Min-Hui Lo[1], Chia Chou[1,2], and Sanjiv Kumar[3]

[1]Department of Atmospheric Sciences, National Taiwan University, Taipei, Taiwan, [2]Research Center for Environmental Changes, Academia Sinica, Taipei, Taiwan, [3]Physical Science Division, NOAA Earth System Research Laboratory, Boulder, Colorado, USA

Key Points:
- A higher frequency of intense precipitation events is observed for the Maritime Continent
- More extreme precipitation in the Maritime Continent leads to a reduced groundwater recharge
- Intensified water cycle has potential to result in a strong temporal heterogeneity in soil water

Supporting Information:
- Supporting Information S1

Corresponding author:
M.-H. Lo, minhuilo@ntu.edu.tw

Citation:
Lan, C.-W., M.-H. Lo, C. Chou, and S. Kumar (2016), Terrestrial water flux responses to global warming in tropical rainforest areas, *Earth's Future*, *4*, 210–224, doi:10.1002/2015EF000350.

Received 30 DEC 2015
Accepted 14 APR 2016
Accepted article online 19 APR 2016
Published online 18 MAY 2016

© 2016 The Authors.

This is an open access article under the terms of the Creative Commons Attribution-NonCommercial-NoDerivs License, which permits use and distribution in any medium, provided the original work is properly cited, the use is non-commercial and no modifications or adaptations are made.

Abstract Precipitation extremes are expected to become more frequent in the changing global climate, which may considerably affect the terrestrial hydrological cycle. In this study, Coupled Model Intercomparison Project Phase 5 archives have been examined to explore the changes in normalized terrestrial water fluxes (precipitation minus evapotranspiration minus total runoff, divided by the precipitation climatology) in three tropical rainforest areas: Maritime Continent, Congo, and Amazon. Results show that a higher frequency of intense precipitation events is predicted for the Maritime Continent in the future climate than in the present climate, but not for the Amazon or Congo rainforests. Nonlinear responses to extreme precipitation lead to a reduced groundwater recharge and a proportionately greater amount of direct runoff, particularly for the Maritime Continent, where both the amount and intensity of precipitation increase under global warming. We suggest that the nonlinear response is related to the existence of a higher near-surface soil moisture over the Maritime Continent than that over the Amazon and Congo rainforests. The wetter soil over the Maritime Continent also leads to an increased subsurface runoff. Thus, increased precipitation extremes and concomitantly reduced terrestrial water fluxes lead to an intensified hydrological cycle for the Maritime Continent. This has the potential to result in a strong temporal heterogeneity in soil water distribution affecting the ecosystem of the rainforest region and increasing the risk of flooding and/or landslides.

1. Introduction

This study investigates changes in the normalized terrestrial water fluxes (TWFn) defined as precipitation minus evapotranspiration minus total runoff, divided by the precipitation climatology, under the global warming scenarios in three tropical rainforest areas: Maritime Continent, Congo, and Amazon. A number of studies have suggested significant changes in the hydrological cycle and the precipitation extremes under the global warming scenarios (reviewed later). None of these studies were focused on the tropical rainforest areas. Tropical rainforests are crucial in altering water and carbon cycles of the earth. Changes in tropical precipitation, land-use management, and deforestation affect the rainforest ecosystems by altering the hydrological cycle and surface energy balance [*Kumagai et al.*, 2004; *Malhi et al.*, 2011; *Reynolds et al.*, 2011; *Malhi et al.*, 2013; *Banin et al.*, 2014; *Brienen et al.*, 2015; *Lawrence and Vandecar*, 2015]. Tropical deforestation also influences the precipitation in the extra-tropics through atmospheric teleconnection processes [*Dominguez et al.*, 2008; *Lawrence and Vandecar*, 2015]. Climate model simulations suggest increased productivity (growth rate) of the rainforests under the elevated carbon dioxide concentration [*Malhi and Grace*, 2000; *Phillips et al.*, 2007]. However, the question of how changes in precipitation extremes affect terrestrial water fluxes (TWF) (precipitation minus evapotranspiration minus total runoff) in tropical rainforest areas are not well investigated. Below here, we first review the literature on the effects of global warming on the hydrological cycle, and precipitation extremes and other related work that leads to this study. Data and methods are presented in Sections 2 and 3, respectively, followed by results in Section 4. Conclusions from this study are presented in Section 5.

Increasing anthropogenic carbon dioxide emissions have caused an increase in the surface and atmospheric temperature and consequently an increase in the atmospheric water vapor concentration at the rate of 7%/K in accordance with the Clausius–Clapeyron relationship [*Trenberth et al.*, 2003; *Held and Soden*, 2006; *Santer et al.*, 2007; *Vecchi and Soden*, 2007; *Allan and Soden*, 2008]. Studies that have analyzed the observations and model simulations have found that wet and warm regions are becoming wetter [*Held and Soden*, 2006;

Zhang et al., 2007; *Chou and Lan*, 2012; *Chou et al.*, 2013; *Tan et al.*, 2015]. Recent studies [e.g., *Greve et al.*, 2014; *Greve and Seneviratne*, 2015] have found uncertainties in future projections of wet and dry regions that can be related to the internal climate variability and water limitations to evaporation over land [*Kumar et al.*, 2015]. *Byrne and O'Gorman* [2015] suggested that the gradients of near-surface warming, e.g., polar amplification and greater warming over land than oceans lead to a drying tendency over the land. Overall, the water resource management is expected to become increasingly critical especially in high-risk regions, e.g., warm and wet tropical rainforest regions (discussed later).

Seasonal shift in precipitation and changes in precipitation extremes are more critical than the changes in mean precipitation [e.g., *Trenberth et al.*, 2003; *Chou et al.*, 2013], because the seasonal shift and the extreme events cause more societal damages [*Zhang et al.*, 2011; *Intergovernmental Panel on Climate Change*, 2012]. Previous studies have found that both the intensity and frequency of heavy rainfall events are likely to increase under the global warming [*Trenberth et al.*, 2003; *Sun et al.*, 2007; *Allan and Soden*, 2008; *Liu et al.*, 2009; *O'Gorman and Schneider*, 2009; *Chen et al.*, 2012]. The global warming also increases the annual range of precipitation (maximum minus minimum monthly precipitation), which is attributed to the thermodynamics associated with the changes in water vapor concentration [*Chou and Lan*, 2012; *Chou et al.*, 2013].

Increasing temperature and precipitation extremes can substantially alter the terrestrial water cycle, for example, by causing alterations in soil water storage and runoff [*Dirmeyer et al.*, 2014; *Huang et al.*, 2014; *Kumar et al.*, 2014; *Zhang et al.*, 2014; *Wu et al.*, 2015]. The global average dry conditions, and drought areas are likely to enlarge under the global warming [*Dai*, 2011; 2012; *Sheffield et al.*, 2012; *Cook et al.*, 2015; *Zhao and Dai*, 2015]. The relative change in runoff can be considerably larger than that of precipitation because of nonlinear runoff responses to the precipitation intensity [*Huang et al.*, 2014]. Such changes in runoff may result in a higher risk of flooding that can cause frequent landslides, and reduction in productivity because of changes in the erosion rate [*Nearing et al.*, 2004; *Huang et al.*, 2006]. In south Asia, climate models' projections show that the annual mean river flow may double by the end of the twenty-first century; while simultaneously the areas experiencing severe water scarcity may also increase because of increasing irrigation and population demands [*Mathison et al.*, 2015].

Kumar et al. [2014] employed available water (AW) index (precipitation minus evapotranspiration, divided by the precipitation climatology) to investigate future trends and seasonal changes of water availability in the twenty-first century based on 20 models in the Coupled Model Intercomparison Project Phase 5 (CMIP5) archives. Results showed that dry seasons are predicted to become drier and wet seasons become wetter for the most of the world [*Kumar et al.*, 2014]. Typically, total water storage includes water stored in snow, soil layers, and in the groundwater aquifers. The total water storage can sustain tree growth by supplying water from deeper soil layers and groundwater reservoirs. Changes in the total water storage affect the amount of groundwater-produced runoff or the subsurface runoff [e.g., *Lo et al.*, 2008], which will be a vital water resource in the future. *Wu et al.* [2015] found that the annual range of soil moisture increases under the global warming because of substantial declines in snowfall and increased rainfall over the middle and high latitudes regions of the Northern Hemisphere. However, none of the above studies were focused on the tropical rainforest regions.

2. Data

We analyze monthly CMIP5 model outputs from historical simulations from 1900 to 2005, and Representative Concentration Pathway 8.5 (RCP8.5) simulations of the future-warming scenario from 2006 to 2100, which corresponds to a radiative forcing of 8.5 W per square meter in 2100 (relative to that of the preindustrial period) [*Taylor et al.*, 2012]. Twelve climate models (Table 1) are used in this study, and only one ensemble member from each model is used. We employ these 12 climate models because only these models have all required data (precipitation, evapotranspiration, total runoff, and surface runoff) available. All model outputs are interpolated to 1° by 1° (360 × 180 grids) using bilinear interpolation. We estimate trends from 1981 to 2100 locally (grid box) using regression-based linear trend estimator. Note that we focus on monthly precipitation extremes in this study.

In addition, we also compare TWFn from CMIP5 and observations. We use monthly gridded gauge-analysis precipitation data from Global Precipitation Climate Center (GPCC), which is derived from quality-controlled

Table 1. CMIP5 Models From Historical and RCP8.5 Scenario Data Used in This Study

	Model	Institution	Resolution
1	CanESM2	CCCma	128 × 64
2	CCSM4	NCAR	288 × 192
3	CESM1-CAM5	NSF-DOE-NCAR	288 × 192
4	CSIRO-Mk3.6.0	CSIRO-QCCCE	192 × 96
5	GFDL-CM3	NOAA GFDL	144 × 90
6	GFDL-ESM2G	NOAA GFDL	144 × 90
7	GFDL-ESM2M	NOAA GFDL	144 × 90
8	GISS-E2-R	NASA GISS	144 × 90
9	INM-CM4	INM	180 × 120
10	MIROC5	MIROC	128 × 64
11	MIROC-ESM	MIROC	128 × 64
12	MPI-ESM-LR	MRI	192 × 96

CMIP5, Coupled Model Intercomparison Project Phase 5; RCP8.5, Representative Concentration Pathway 8.5.

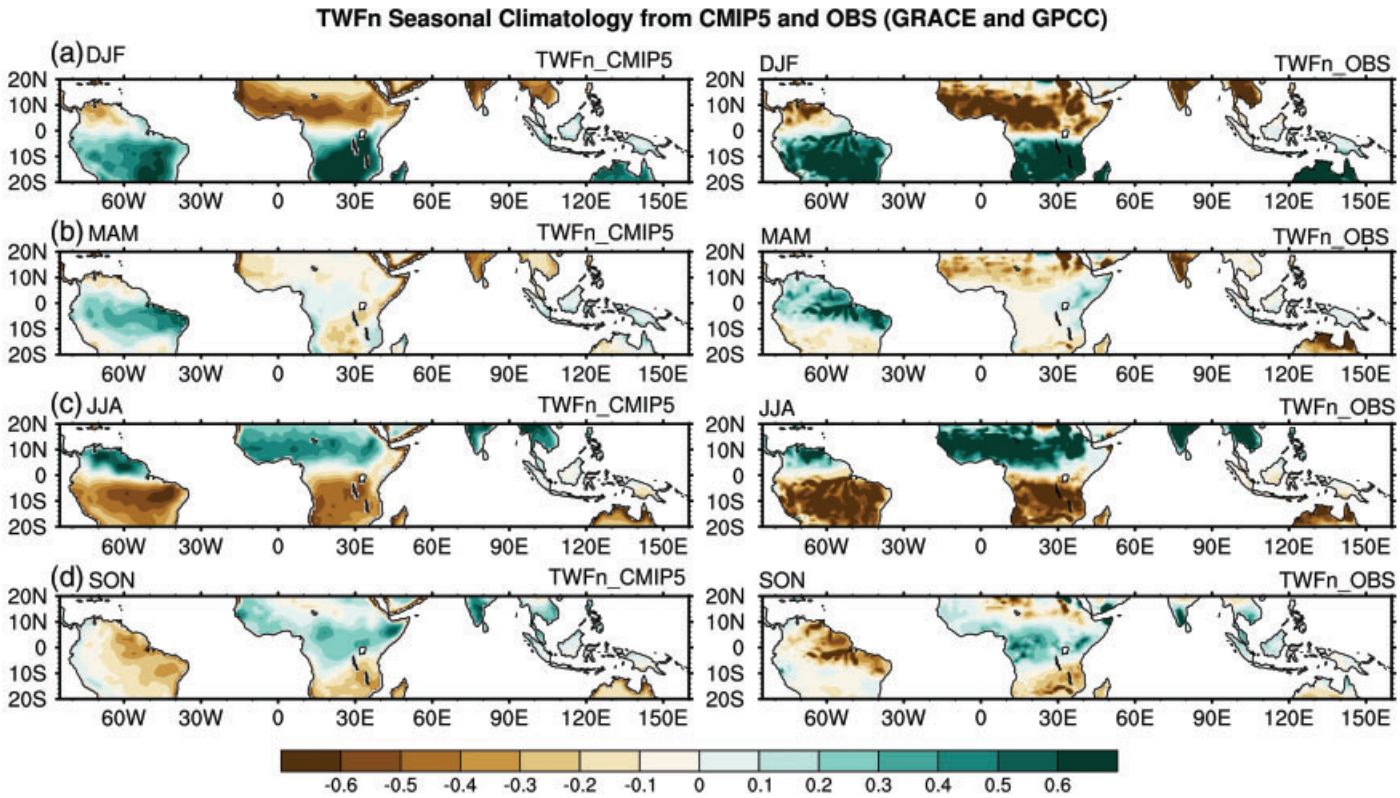

Figure 1. Seasonal climatology related to (1) TWFn_CMIP5, normalized terrestrial water fluxes (TWFn) in the Coupled Model Intercomparison Project Phase 5 (CMIP5) 12-model ensemble mean from 1981 to 2005 and (2) TWFn_OBS, TWFn from GRACE total water storage, and GPCC climatology precipitation data from 2003 to 2013.

station data [*Rudolf et al.*, 2010], and total water storage variations from Gravity Recovery and Climate Experiment (GRACE) [*Tapley et al.*, 2004] from 2003 to 2013. Recent releases (RL05) of GRACE data [*Landerer and Swenson*, 2012] from the Center for Space Research at the University of Texas at Austin are used in this study. Our analyses are focused on the Amazon, Congo, and Maritime Continent tropical rainforest areas. Total runoff integrating pathways data on a 1° grid [*Oki and Sud*, 1998] provide basin boundaries for the Amazon and the Congo. All land area within 10°S–10°N and 90°W–150°W are considered as the Maritime Continent (Figure 2).

Table 2. The Seasonal Climatology Mean Bias of TWFn and $P-E-R$ From CMIP5 Simulations Compared to TWFn_OBS From GRACE and GPCC, and $P-E-R$ From Monthly Difference of GRACE in the Tropics (20°S–20°N)

	$P-E-R$	TWFn
Dec, Jan, Feb	−3.81	−0.08
Mar, Apr, May	−0.51	0.03
Jun, Jul, Aug	2.46	−0.11
Sep, Oct, Nov	5.17	−0.01

CMIP5, Coupled Model Intercomparison Project Phase 5; GPCC, Global Precipitation Climate Center; GRACE, Gravity Recovery and Climate Experiment; TWFn, normalized terrestrial water fluxes.

3. Methodology

3.1. Normalized Terrestrial Water Fluxes From CMIP5 and Observations

We calculate a TWFn for each month in a given year as follows:

$$\mathrm{TWFn}_{m,y} = \left(P_{m,y} - \mathrm{ET}_{m,y} - R_{m,y}\right) \times \frac{1}{\overline{P}} = \frac{dS}{dt} \times \frac{1}{\overline{P}} \tag{1}$$

where $\mathrm{TWFn}_{m,y}$ is the TWFn, $P_{m,y}$ is the precipitation, $\mathrm{ET}_{m,y}$ is the evapotranspiration, $R_{m,y}$ is the total runoff, $\overline{P}$ is the precipitation climatology in the historical period from 1981 to 2005 in the respective models' climate simulations, and dS/dt represents the rate of change in total water storage (s). Subscripts m and y represent each year and month. This index is similar to the AW index, $\mathrm{AW}_{m,y} = (P_{m,y} - \mathrm{ET}_{m,y})/\overline{P}$ used by *Kumar et al.* [2014], but TWFn additionally considers the effects of total runoff. Thus, the TWFn can be regarded as the net water flux (as the fraction of mean precipitation) into the land water storage (i.e., groundwater). Normalization of terrestrial water flux allows a comparison to regions with different precipitation climatologies, reducing uncertainties in TWF because of the biases of precipitation in the climate models [*Sheffield et al.*, 2013], and allows us to assess the annual range between different seasons [*Kumar et al.*, 2014]. We also evaluate the TWFn using GRACE land water storage monthly changes (dS/dt) and GPCC precipitation climatology ($\overline{P}$) data from 2003 to 2013.

3.2. Atmospheric Moisture Budget Analysis

The atmospheric moisture budget analysis can be used to investigate the thermodynamic and dynamic contribution to precipitation changes under the global warming scenarios [*Held and Soden*, 2006; *Chou et al.*, 2009; *Seager et al.*, 2010]. We use vertically integrated moisture budget analysis [*Chou and Lan*, 2012] to investigate why monthly precipitation probability density function (PDF) shifted toward higher intensity over the Maritime Continent. For long-term averages, the time derivative term of specific humidity can be ignored, and the moisture budget can be written as follows:

$$P - E = -\nabla \cdot \mathbf{F} = -\langle \nabla \times (\mathbf{V}q) \rangle \tag{2}$$

where P indicates the precipitation, E is the evaporation, $\mathbf{F}$ is column-integrated moisture flux, $\mathbf{V}$ indicates the total wind field, comprising the $\mathbf{u}$, $\mathbf{v}$, and ω components, and $\langle\ \rangle$ denotes a mass integration throughout the troposphere. Because the pressure velocity is near zero at the surface and the tropopause [*Tan et al.*, 2008], $-\langle q\nabla \cdot \mathbf{V} \rangle$ is approximately zero and $-\langle \mathbf{V} \cdot \nabla q \rangle$ can be further decomposed to the horizontal moisture advection component ($-\langle \mathbf{V_h} \cdot \nabla q \rangle$) and vertical moisture advection component ($-\langle \omega \partial_p q \rangle$) . The term $\mathbf{V_h}$ indicates the horizontal wind field, including the $\mathbf{u}$ and $\mathbf{v}$ components, and ω indicates pressure velocity. Therefore, the vertically integrated moisture budget equation can be written as follows [*Chou and Neelin*, 2004]:

$$P \approx -\langle \mathbf{V_h} \cdot \nabla q \rangle - \langle \omega \partial_p q \rangle + E + \mathrm{res.} \tag{3}$$

The vertical moisture advection ($-\langle \omega \partial_p q \rangle$) is the part of the convergence of moisture flux induced by vertical motion or low-level convergence. The term $-\langle \mathbf{V_h} \cdot \nabla q \rangle$ in equation (3) is the horizontal moisture advection, which is the part of the convergence of moisture flux related to horizontal velocity. The final term res. in equation (3) is a residual term that includes transient eddies and nonlinear effects. All units in equations (2) and (3) are Watts per square meter, and are divided by 28 to yield values in millimeter per day. In the vertical

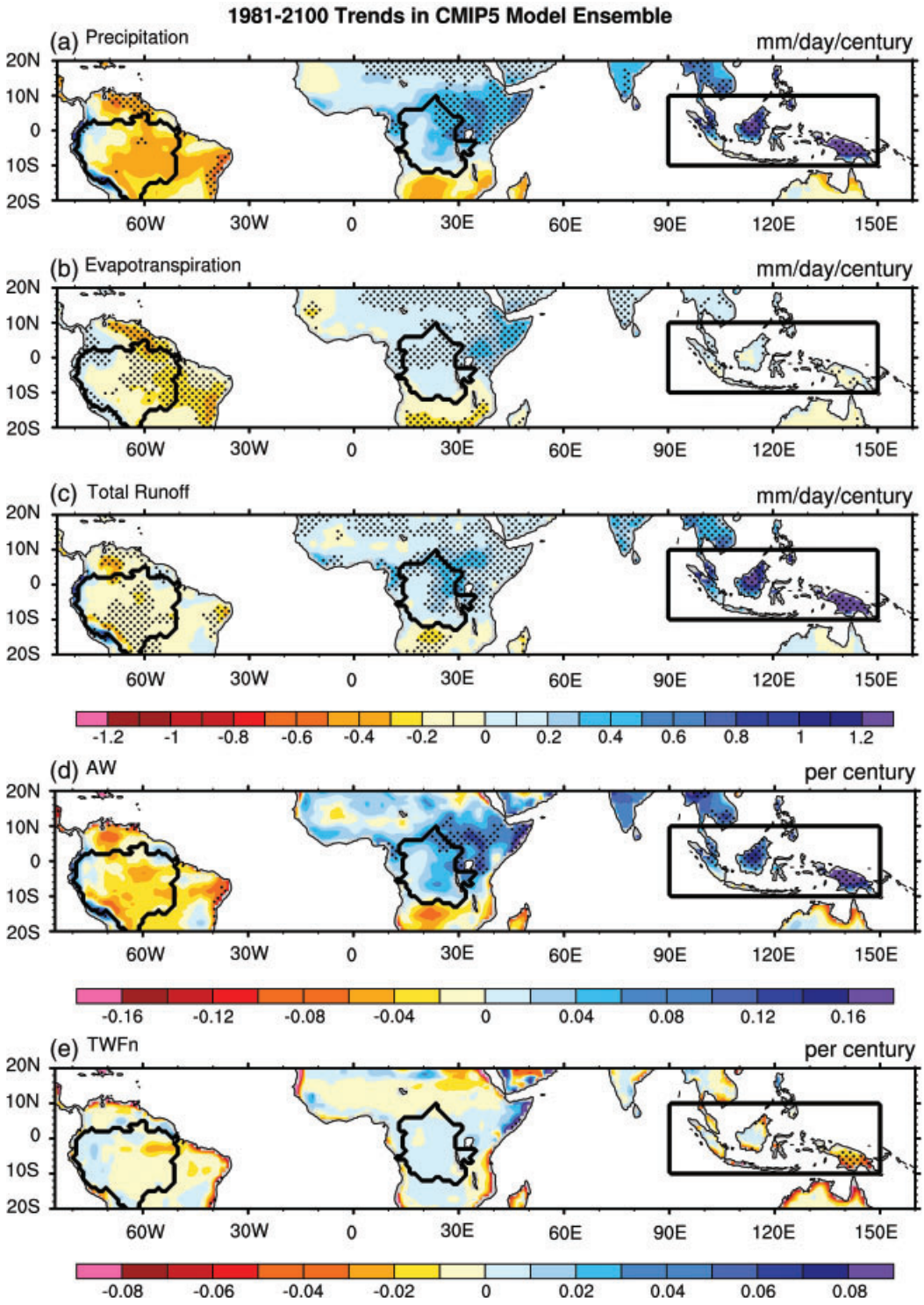

Figure 2. Spatial distributions of the linear trend from 1981 to 2100 from the Coupled Model Intercomparison Project Phase 5 (CMIP5) 12-model ensemble mean (one run from each model) for three tropical rainforests in (a) precipitation, (b) evapotranspiration, (c) total runoff, (d) available water (AW), and (e) normalized terrestrial water flux (TWFn). The black solid contour lines represent the Amazon, Congo, and Maritime Continent rainforests. The trends that passed the 95% statistical confidence level of a Student's *t*-test are stippled.

Table 3. CMIP5 12-Model Ensemble Mean of Areas Percentage Where $P' > 0$ and $AW' < 0$, $P' > 0$ and $TWFn' < 0$, and $R' > P' > 0$ in Three Tropical Rainforests

%	Amazon	Congo	Maritime Continent
$P' > 0$ and $AW' < 0$	3.40	0.98	3.01
$P' > 0$ and $TWFn' < 0$	2.20	13.77	66.54
$R' > P' > 0$	0.20	2.30	57.89

P', AW', $TWFn'$, and R' individually indicate the trends of precipitation, AW, TWFn, and total runoff during 1981–2100.
AW, available water; CMIP5, Coupled Model Intercomparison Project Phase 5.

moisture advection term of equation (3), $\boldsymbol{\omega}$ and q can be separated from current climate, i.e., $\boldsymbol{\omega} = \overline{\boldsymbol{\omega}} + \boldsymbol{\omega}'$ and $q = \overline{q} + q'$, where $(^{-})$ is the current climate from the average of 1981–2005 in historical simulations of the CMIP5 archive, and $(')$ is the departure from the current climate. Therefore, the vertical moisture advection term can be further decomposed into the four terms:

$$-\langle \boldsymbol{\omega} \partial_p q \rangle \approx -\langle \overline{\boldsymbol{\omega}} \partial_p \overline{q} \rangle - \langle \overline{\boldsymbol{\omega}} \partial_p q' \rangle - \langle \boldsymbol{\omega}' \partial_p \overline{q} \rangle - \langle \boldsymbol{\omega}' \partial_p q' \rangle \quad (4)$$

In equation (4), the nonlinear term $\langle \boldsymbol{\omega}' \partial_p q' \rangle$ is disregarded in this study. The term $-\langle \overline{\boldsymbol{\omega}} \partial_p q' \rangle$ in equation (4) is associated with changes in water vapor, which is mainly induced by temperature changes and commonly termed as the thermodynamic component [*Held and Soden*, 2006; *Chou et al.*, 2009; *Seager et al.*, 2010]. The third term on the right side of equation (4) is associated with changes in vertical velocity, related to tropical circulation; therefore, it is termed the dynamic component [*Held and Soden*, 2006; *Chou et al.*, 2009; *Seager et al.*, 2010]. In addition, the precipitation, horizontal moisture advection, and evaporation terms can also be decomposed to current climate and departure from the current climate components. Thus, the precipitation changes can be written as follows:

$$P' \approx -\langle \mathbf{V_h} \cdot \nabla q \rangle' - \langle \overline{\boldsymbol{\omega}} \partial_p q' \rangle - \langle \boldsymbol{\omega}' \partial_p \overline{q} \rangle + E' + \text{res.} \quad (5)$$

and

$$\overline{P} = -\langle \overline{\mathbf{V_h}} \cdot \nabla \overline{q} \rangle - \langle \overline{\boldsymbol{\omega}} \partial_p \overline{q} \rangle + \overline{E}$$

In this study, we use equation (5) to investigate which component is the main role in inducing the shifts in monthly precipitation spectra to higher intensity over the Maritime Continent.

4. Results

Figure 1 shows the TWFn from the CMIP5 12-model ensemble mean, as well as the TWFn derived from GRACE and GPCC data from the three tropical areas in four seasons. The TWFn comparisons between the CMIP5 data of the historical run and the GRACE and GPCC data are consistent (Figures 1a–1d), because the GRACE data are used to determine the water budget balance between precipitation, evapotranspiration, and total runoff. In addition, Table 2 shows that the mean biases in the CMIP5 TWFn over the tropics (20°S–20°N) are small (from −0.11 to 0.03 at different seasons) when compared to GRACE/GPCC-based TWFn. A slightly smaller amplitude in CMIP5 than observations is consistent with the spatial pattern of TWFn seasonal climatology shown in Figure 1. Thus, we further use the TWFn to describe the changes in terrestrial hydrological responses to global warming for the rainforest areas.

Figure 2 shows the spatial distribution of the linear trend from 1981 to 2100 for precipitation, evapotranspiration, total runoff, and TWFn in the tropics including three tropical rainforest regions outlined by black lines. We also show trends in AW to compare with trends in TWFn. Precipitation increases over the Maritime Continent and Congo, but mostly declines over the Amazon. The trends in evapotranspiration and total runoff are similar to the trend in precipitation in the three rainforests, except for that in Papua New Guinea. This result indicates that the precipitation changes may play a major role that increases runoff and evapotranspiration over the tropics. In addition, the trends in the TWFn are generally smaller than that of the AW; the trends over the Maritime Continent differ the most (Figure 2e), where the trend in the TWFn even

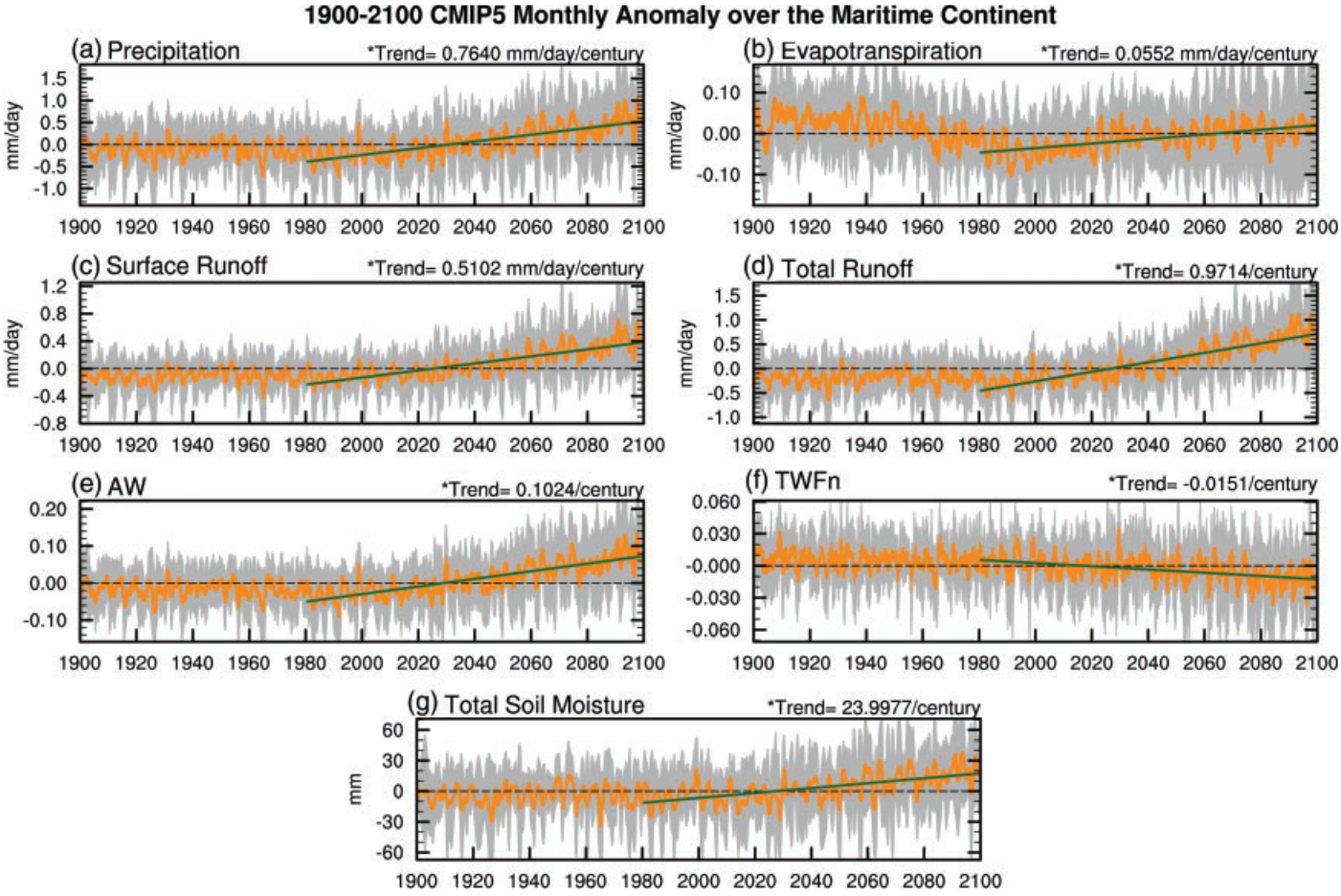

Figure 3. Anomaly time series (1900–2100) of 12 Coupled Model Intercomparison Project Phase 5 (CMIP5) model means of (a) precipitation, (b) evapotranspiration, (c) surface runoff, (d) total runoff, (e) available water (AW), (f) normalized terrestrial water fluxes (TWFn), and (g) total soil moisture averaged for the Maritime Continent. The green line denotes the linear trend from 1981 to 2100, the gray shading is the mean ± one standard deviation for the regional average series of the 12 CMIP5 models, and the orange line is the 12 CMIP5 model means with the 12-month running mean.

becomes negative. This implies that the net fluxes of water into soil and ground water become smaller for the Maritime Continent as the climate warms, despite the rainforest becoming wetter (positive trend of AW index) and more precipitation. This result also indicates that changes in total runoff may be more critical for the Maritime Continent than that for the Amazon and Congo.

Table 3 shows that few regions (in area percentages) have decreased AW trends and increased precipitation trends ($P' > 0$ and $AW' < 0$). The area percentages are approximately 3%, 1%, and 3% over the Amazon, Congo, and Maritime Continent, respectively. In other words, few regions have evapotranspiration trends exceeding precipitation trends. However, the area percentage that exhibit a negative TWFn trend and a positive precipitation trend is markedly higher in the Maritime Continent (67%) than that in the other two rainforests (2% in the Amazon and 14% in the Congo). The area percentage of with $R' > P' > 0$ is also higher in the Maritime Continent than other two rainforests in terms of ensemble mean. An analysis of individual climate model simulations shows that 8 of 12 models have the largest area percentage of $P' > 0$ and $TWFn' < 0$, or of $R' > P' > 0$ in the Maritime Continents (Table S1, Supporting Information). Hence, the greater increase in the total runoff trend than the increasing precipitation trends leads to the negative trend in the TWFn for the Maritime Continent.

Figure 3 presents the anomaly time series of the 12 CMIP5 model means of precipitation, evapotranspiration, surface runoff, total runoff, AW, TWFn, and total soil moisture from 1900 to 2100 averaged for the Maritime Continent. Most time series, except for that of TWFn, exhibit clear increasing trends from 1981 to 2100. The increasing trends of precipitation, evapotranspiration, and total runoff from 1981 to 2100

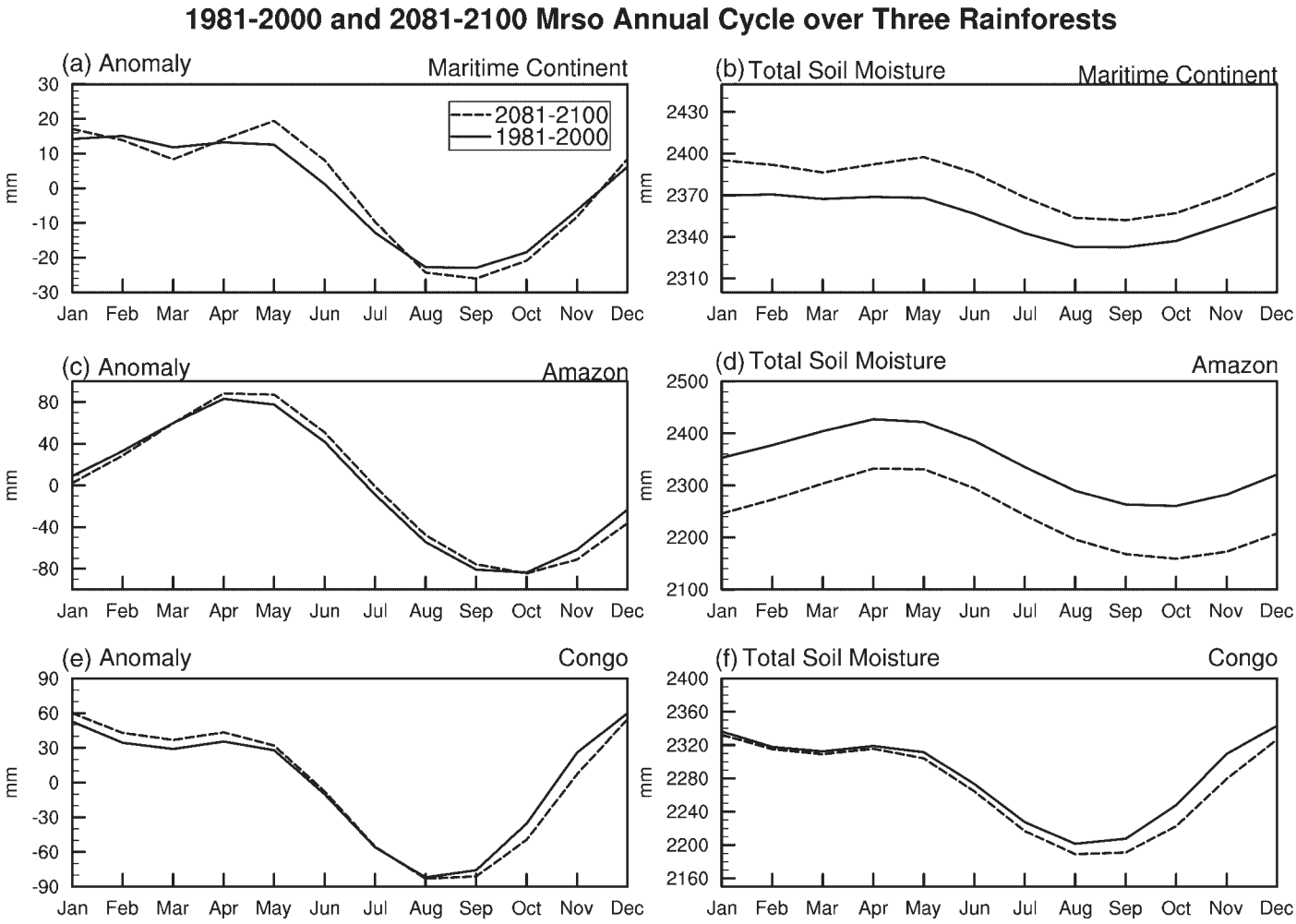

Figure 4. The averaged seasonal cycle of total soil moisture from the Coupled Model Intercomparison Project Phase 5 (CMIP5) 12-model ensemble mean during 1981–2000 and 2081–2100 for anomaly and absolute value over the (a, b) Maritime Continent, (c, d) Amazon, and (e, f) Congo.

are 0.76, 0.06, and 0.97 mm/day/century, respectively (Figures 3a, 3b, and 3d). In addition, AW has a clear increasing trend, implying that the region becomes wetter under global warming (Figure 3e). For the Amazon, although the precipitation decreases from 1981 to 2100, the evapotranspiration and total runoff also decrease, causing an approximately neutral trend in TWFn from 1981 to 2100. Table 3 and Figure 3 indicate that the reduced TWFn under global warming is most likely caused by the stronger increase in the total runoff trend than in the precipitation trend. In addition, the trend of surface runoff for the Maritime Continent also increases, but not to a greater extent than that of precipitation (Figure 3c).

Because the long-term mean of TWFn is positive, the total soil moisture over the Maritime Continent has an increasing trend from 1981 to 2100 (Figure 3g). A difference analysis between the period of 2081–2100 and the period of 1981–2000 shows that the soil moisture in the Maritime Continent becomes higher in the future (Figure 4b), the soil moisture becomes lower over the Amazon (Figure 4d), and near neutral over the Congo (Figure 4f) in terms of seasonal cycle. In addition, the seasonal variability of soil moisture is smaller over the Maritime Continent than the other two rainforest regions because of the smaller precipitation seasonal cycle. However, there is a common feature that the seasonal range of total soil moisture in three regions all become larger, especially for the Maritime Continent (Figures 4a, 4c, and 4e). The seasonal variability or the annual range of soil moisture over the Maritime Continent is much smaller than the other two regions, and that is from the smaller seasonal variability of precipitation. The amount of soil water is higher over the Maritime Continent regions; thus, no obvious dry season is shown over the Maritime continent so that there is a longer growing season for the trees over the Maritime Continent. That's the major reason that

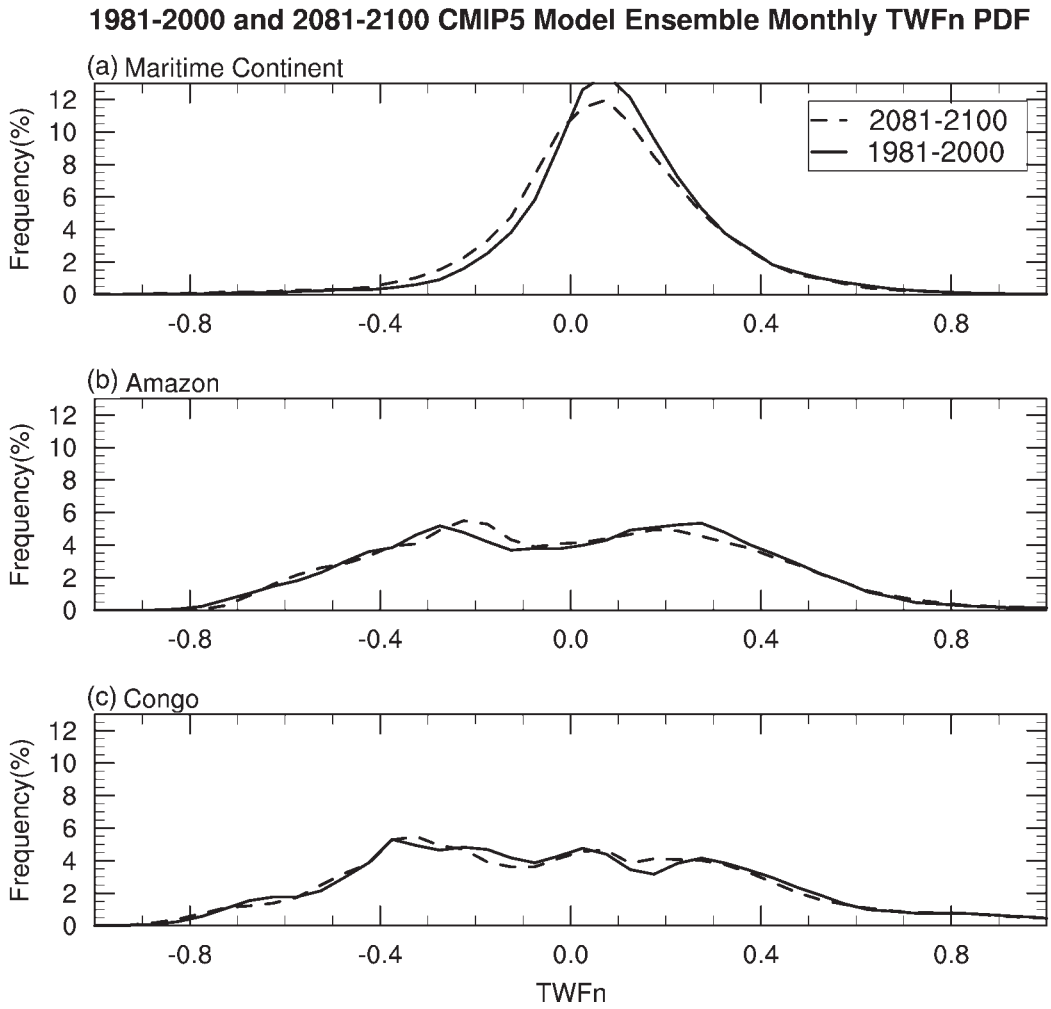

Figure 5. The probability density function of monthly normalized terrestrial water fluxes (TWFn) from the Coupled Model Intercomparison Project Phase 5 (CMIP5) 12-model ensemble mean (one run from each model) between 1981–2000 and 2081–2100 averaged for the (a) Maritime Continent, (b) Amazon, and (c) Congo.

the tree's height over the Maritime Continent is higher than that over the other two rainforests [*Banin et al.*, 2014].

Figure 5 shows the monthly TWFn spectra in the CMIP5 12-model ensemble mean during the periods of 1981–2000 and 2081–2100 for the three rainforest areas. Over the Maritime Continent, the negative TWFn value during 2081–2100 has a higher frequency than that during 1981–2000 (approximately 38% higher) when TWFn is less than −0.1 (Figure 5a), but rather similar over the Amazon and Congo rainforests (Figures 5b and 5c). The total soil moisture including liquid water and soil ice has an increasing trend (become wetter) because most of TWFn are positive from 1981 to 2100 over the Maritime Continent so a net increase of water into the land. However, TWFn has a clear decreasing trend from 1981 to 2100 or the negative TWFn becomes more frequent and becomes more negative, implying the duration (magnitude) of losing water from land water storage becomes longer (larger) in the future (Figures 3f, 3g, and 5a).

Because of the nonlinear responses of land hydrological processes to precipitation extremes, runoff can increase exponentially with global warming [*Huang et al.*, 2014]. Also, the stronger precipitation intensity under global warming may induce more surface and subsurface runoff, caused by wetter soil as shown in *Dirmeyer et al.* [2014]. Figure 6 shows the monthly precipitation intensity spectra in the CMIP5 12-model ensemble mean during 1981–2000 and 2081–2100 averaged for the three rainforest areas. The precipitation intensity spectra indicate lighter precipitation for the Amazon compared with that for the Maritime

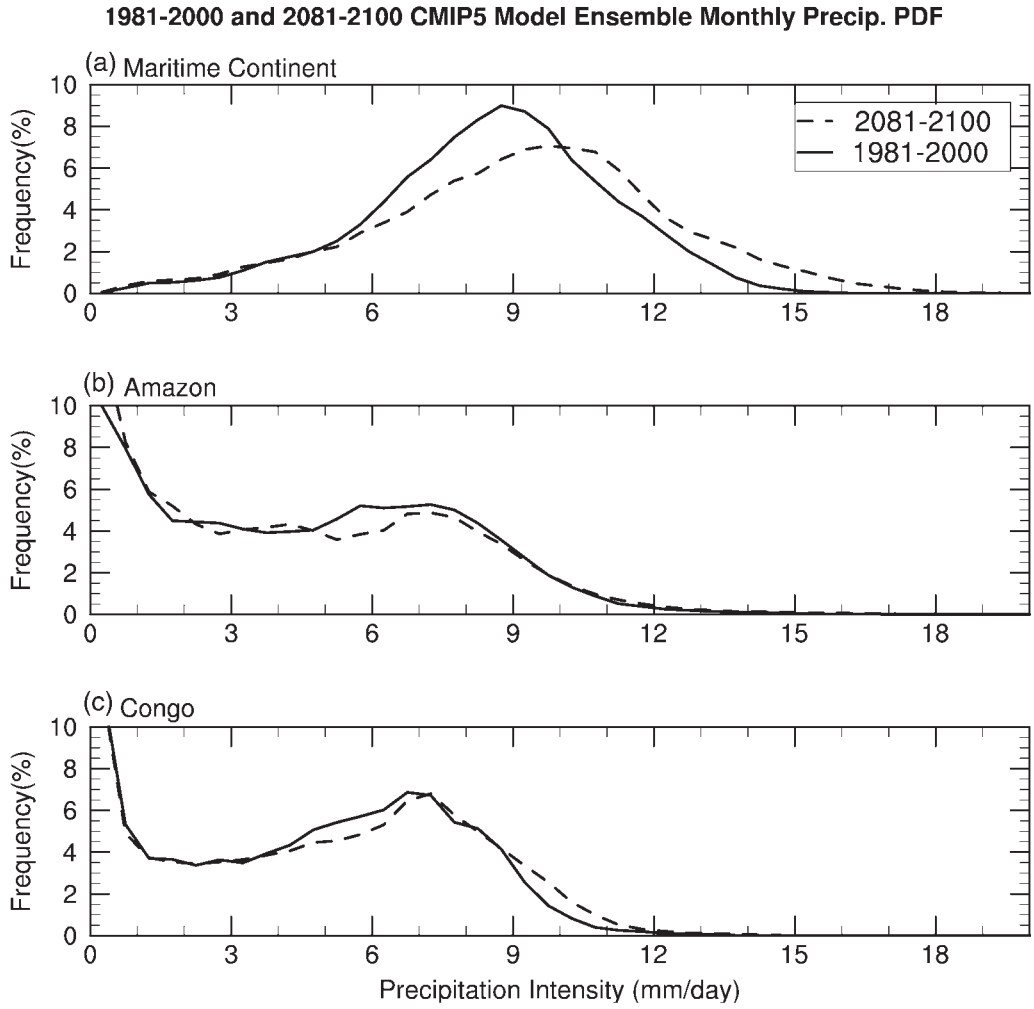

Figure 6. As in Figure 5, but for monthly precipitation.

Continent. Figure 6a clearly shows that the precipitation intensity spectra intensify for the Maritime Continent under global warming. The precipitation intensity spectra, however, remain similar between 1981–2000 and 2081–2100 for the Amazon and Congo (Figures 6b and 6c). Note that Figure 6 shows the result from the 12-model ensemble mean, and we also analyze the precipitation intensity spectra from the individual models (results not shown). Eight of 12 models clearly show the precipitation PDF shifting toward a higher intensity over the Maritime Continents, and the rest of models show the precipitation intensity spectra not changing.

In the Maritime Continent, the runoff ratio (*R*/*P*; the ratio of runoff to precipitation) is high throughout the whole year because of a weak seasonality of precipitation (Figure 7a). For the Amazon and Congo regions, the strong seasonal cycle of *R*/*P* is attributable to the higher precipitation seasonality (Figures 7b and 7c). Figure 7 also indicates that under global warming, the *R*/*P* for the Maritime Continent is approximately 0.5, which is substantially higher than those for the Amazon (0.25–0.5) and Congo (0.2–0.35) regions. The major mechanisms causing the high *R*/*P* are the precipitation extremes as well as the wetter soil for the Maritime Continent (Figure 3g). Increases in rainfall can cause higher water storage, and when the soil becomes wetter or near saturated, the catchment transfers most of the excess rainfall into runoff [*Huang et al.*, 2014] leading to a higher *R*/*P*. Therefore, precipitation extremes lead to more surface runoff for the Maritime Continent. Also, the soil is generally wet, leading to more subsurface runoff and thus a greater *R*/*P* for the Maritime Continent than for other two rainforest regions. Note that the *R*/*P* for the Amazon in the period of 2081–2100

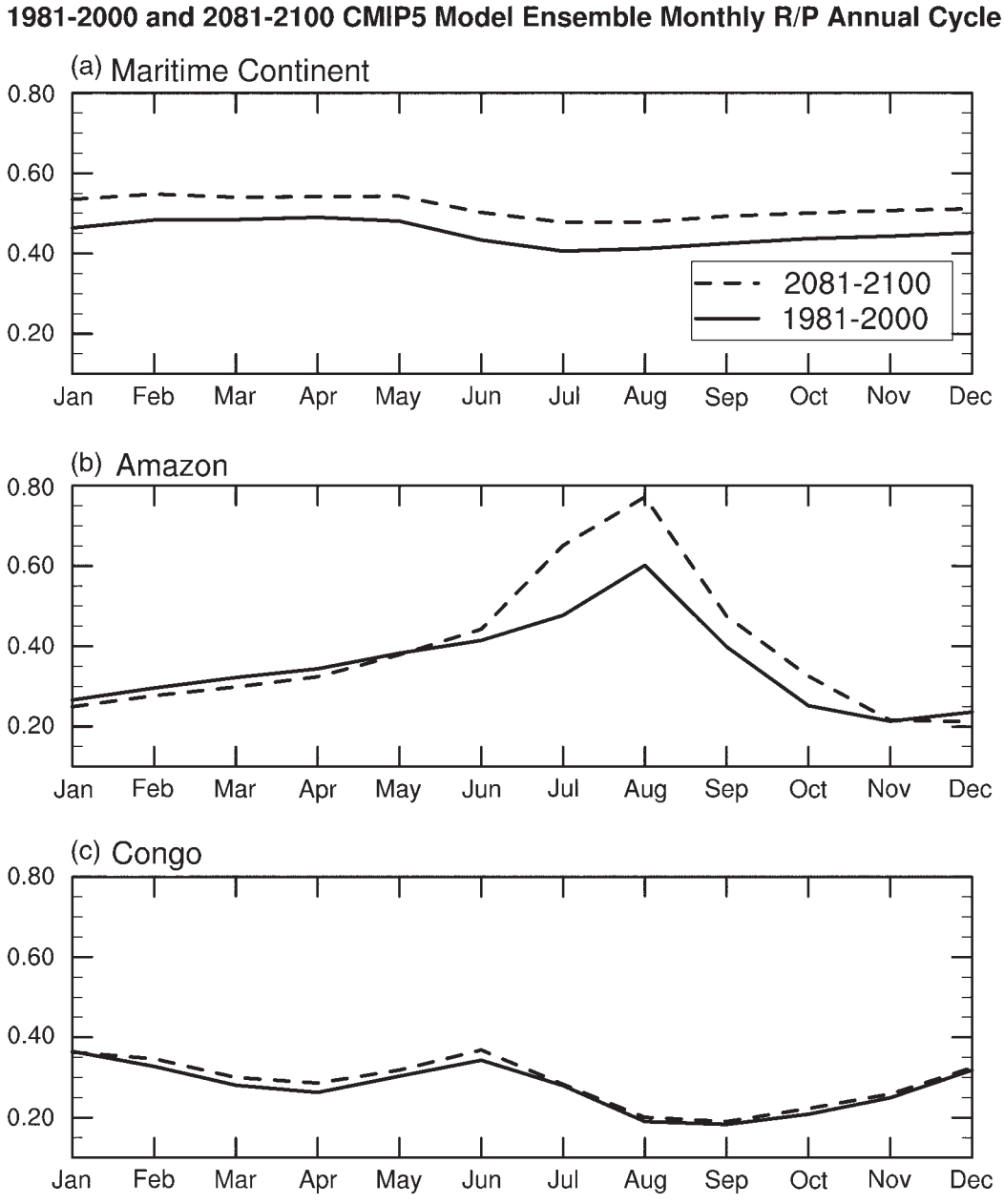

Figure 7. The averaged seasonal cycle of runoff ratio from the Coupled Model Intercomparison Project Phase 5 (CMIP5) 12-model ensemble mean during 1981–2000 and 2081–2100 seasonal averaged for the (a) Maritime Continent, (b) Amazon, and (c) Congo.

indicates dramatic changes from June to September. This is attributable to the low amounts of precipitation and runoff, and with more decreased precipitation than decreased runoff.

We use the vertically integrated moisture budget equation (equations 2–5) to explore the precipitation intensity spectra shifting for the Maritime Continent. Figure 8 shows the comparison of each moisture budget component (i.e., $-\langle \omega \partial_P q \rangle$, $-\langle \mathbf{V_h} \cdot \nabla q \rangle$, and E) between 1981–2000 and 2081–2100 follows precipitation percentile. For example, such as 99th percentile, we calculate each term in the moisture budget when the precipitation intensity at 99% of the cumulated number of precipitation months.

Figure 8a shows that precipitation between two periods have obvious changes in each percentile, especially in a higher percentile (higher than 80%). Based on the moisture budget analysis, the vertical moisture advection term (Figure 8b) has a clear increase when the precipitation intensity is greater than 50%; however, no

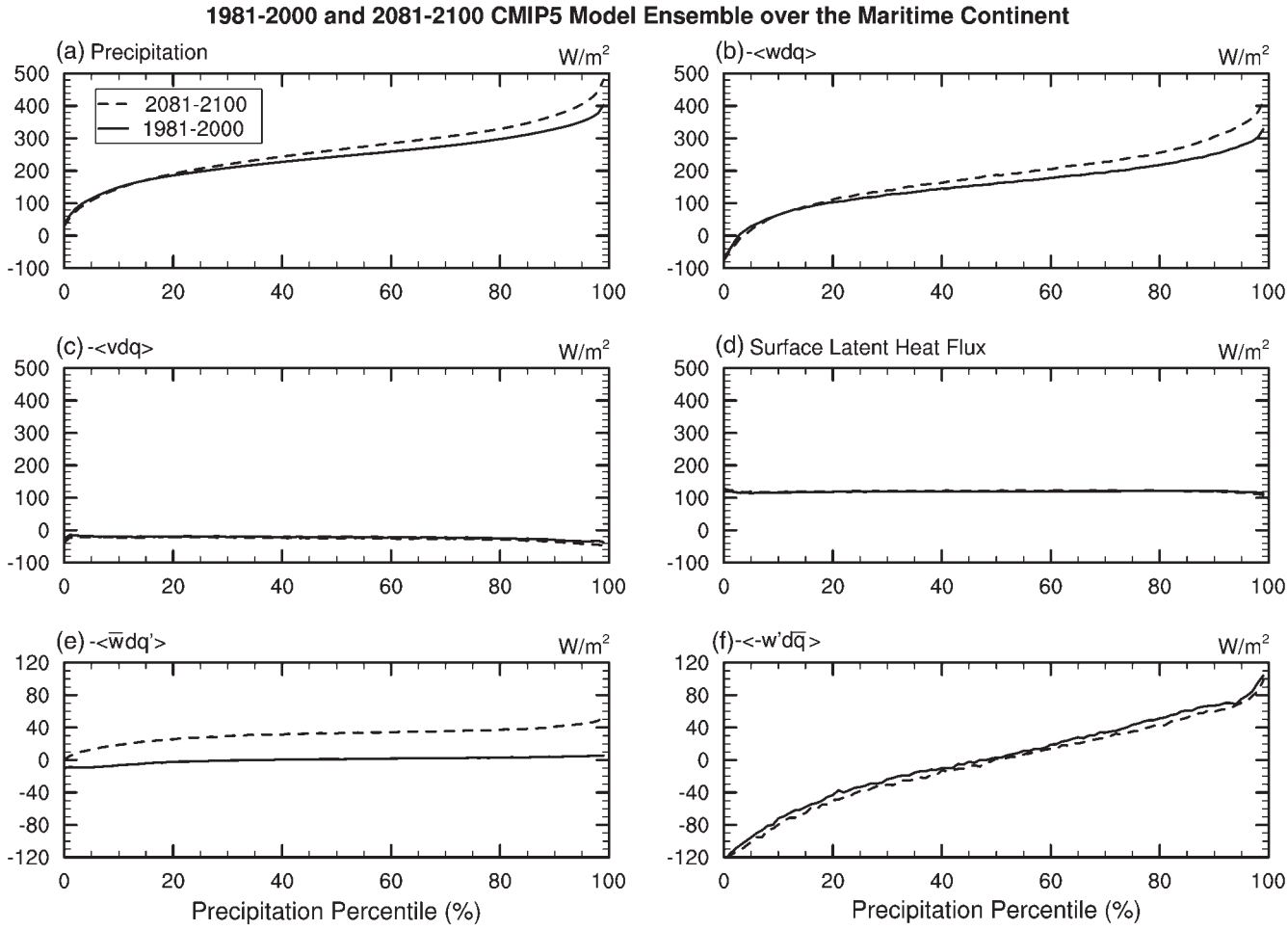

Figure 8. The (a) precipitation, (b) vertical moisture advection, (c) horizontal moisture advection, (d) surface latent heat flux, (e) thermodynamic term of vertical moisture advection, and (f) dynamic term of vertical moisture advection from the Coupled Model Intercomparison Project Phase 5 (CMIP5) 12-model ensemble mean during 1981–2000 and 2081–2100 averaged for the Maritime Continent.

such change occurs for the horizontal moisture advection and latent heat flux terms (Figures 8c and 8d). The vertical moisture advection term can be further decomposed into thermodynamic (water vapor) and dynamic (vertical motion) components. Figures 8e and 8f clearly show that throughout the whole precipitation percentile, the thermodynamic term is higher during 2081–2100 than the present, but such changes are not found in the dynamic component (Figure 8f). The nonlinear term has contributed to changes in the precipitation (Figure S1g); however, the thermodynamic component is the major contribution to the precipitation changes over the Maritime Continent (Figures 8 and S1). For example, the change in thermodynamic component between 2081–2100 and 1981–2000 is approximately 40–50 W/m^2 for the precipitation intensity larger than 50th percentile, while the change in nonlinear term is approximately 0–30 W/m^2 (Figures S1e and S1g). In particular, the contributions from the summation of nonlinear and residual terms are much less than that from the thermodynamic component (Figures S1g and S1h).

Therefore, the increased water vapor under global warming leads to higher thermodynamic contributions to vertical water vapor advection, which is associated with an increase in frequency of extreme precipitation. More precipitation extremes on the wetter soil cause a stronger trends in total runoff than in precipitation, resulting in the declining TWFn trend over the Maritime Continent (Figure 5). Therefore, although the precipitation increases over the Maritime Continent, the net water flux into the land water storage becomes less. That may induce larger annual range of total soil moisture [*Wu et al.*, 2015], increase the risk of flooding and/or landslides, and have impacts on reducing the crop productivity [*Nearing et al.*, 2004; *Huang et al.*, 2006].

5. Summary and Conclusions

We use CMIP5 archives to describe the changes in the TWFn for the three tropical rainforests regions under the global warming. The Amazon and Congo exhibit similar patterns of trends of the AW and TWFn, and their time series have the same tendencies from 1981 to 2100. However, the Maritime Continent shows a declining trend of TWFn, whereas increasing trends are found for all other variables including precipitation, evapotranspiration, surface runoff, total runoff, and AW. This result suggests that a greater changes in the total runoff contribute to a negative TWFn trend over the Maritime Continent. We also found a greater increase (13.45%) in runoff ratio (R/P) over the Maritime Continent than the Amazon (−1.84%) and Congo (7.16%). The larger change in the runoff ratio is attributable to the increase in high intensity precipitation, wetter soil condition, and weak precipitation seasonality over the Maritime Continent. Our results are consistent with the results suggested by *Dirmeyer et al.* [2014], who concluded that increased precipitation extremes could result in increased total runoff. The shift in the precipitation intensity spectra toward higher intensity is associated with the thermodynamics related to the water vapor increasing under global warming. Thus, TWFn has a declining trend from 1981 to 2100 because of increased frequency of high intensity precipitation, and a higher runoff ratio (R/P) over the Maritime Continent. In other words, the negative TWFn becomes more frequent and becomes more negative, implying the duration (magnitude) of losing water from land water storage becomes longer (larger) in the future (Figure 5) that may cause an uneven distribution of water resources. Our study shows the potential vulnerabilities of the Maritime Continent's ecosystem in the changing global climate.

A close agreement (Figure 1 and Table 2) between the CMIP5 model and GRACE/GPCC-based TWFn indicates a reasonable water budget simulations in the models. However, the surface and subsurface runoff parameterizations remain uncertain because of lack of available observations to constrain hydrological simulations in the land surface models [*Lo et al.*, 2008]. While the total runoff is used to calculate the TWFn, the partitioning of surface and subsurface runoff may indirectly affect the TWFn, i.e., changes in surface runoff affect the soil water and thus the evapotranspiration. Such impacts may be more apparent at sub-monthly scale; thus, future research is warranted to determine the changes in this region's precipitation extremes (especially using daily precipitation data to explore the spectral changes) as well as its mechanisms and resulting changes in hydrologic and hydroclimatic responses.

Acknowledgments

We thank editor and two anonymous reviewers for their valuable suggestions for greatly improving the manuscript. We acknowledge the World Climate Research Programme's Working Group on Coupled Modelling, which is responsible for CMIP, and we thank the climate modeling groups for producing and making available their model output. For CMIP, the U.S. Department of Energy's Program for Climate Model Diagnosis and Intercomparison provides coordinating support and led development of software infrastructure in partnership with the Global Organization for Earth System Science Portals. GRACE land data were processed by Sean Swenson, supported by the NASA MEaSUREs Program, and are available at http://grace.jpl.nasa.gov. This study was supported by the MOST 103-2111-M-002-006 to National Taiwan University. Sanjiv Kumar's contribution was supported by NRC Research Associateship Award at NOAA ESRL Physical Science Division.

References

Allan, R. P., and B. J. Soden (2008), Atmospheric warming and the amplification of precipitation extremes, *Science*, *321*(5895), 1481–1484, doi:10.1126/science.1160787.

Banin, L., et al. (2014), Tropical forest wood production: a cross-continental comparison, *J. Ecol.*, *102*(4), 1025–1037, doi:10.1111/1365-2745.12263.

Brienen, R. J., et al. (2015), Long-term decline of the Amazon carbon sink, *Nature*, *519*(7543), 344–348, doi:10.1038/nature14283.

Byrne, M. P., and P. A. O'Gorman (2015), The response of precipitation minus evapotranspiration to climate warming: why the "wet-get-wetter, dry-get-drier" scaling does not hold over land, *J. Clim.*, *28*(20), 8078–8092, doi:10.1175/jcli-d-15-0369.1.

Chen, C.-A., C. Chou, and C.-T. Chen (2012), Regional perspective on mechanisms for tropical precipitation frequency and intensity under global warming, *J. Clim.*, *25*(24), 8487–8501, doi:10.1175/jcli-d-12-00096.1.

Chou, C., and C.-W. Lan (2012), Changes in the annual range of Pprecipitation under global warming, *J. Clim.*, *25*(1), 222–235, doi:10.1175/jcli-d-11-00097.1.

Chou, C., and J. D. Neelin (2004), Mechanisms of global warming impacts on regional tropical precipitation, *J. Clim.*, *17*, 2688–2701, doi:10.1175/1520-0442(2004)017<2688:mogwio>2.0.co;2.

Chou, C., J. D. Neelin, C.-A. Chen, and J.-Y. Tu (2009), Evaluating the "rich-get-richer" mechanism in tropical precipitation change under global warming, *J. Clim.*, *22*(8), 1982–2005, doi:10.1175/2008jcli2471.1.

Chou, C., J. C. H. Chiang, C.-W. Lan, C.-H. Chung, Y.-C. Liao, and C.-J. Lee (2013), Increase in the range between wet and dry season precipitation, *Nat. Geosci.*, *6*(4), 263–267, doi:10.1038/ngeo1744.

Cook, B. I., T. R. Ault, and J. E. Smerdon (2015), Unprecedented 21st century drought risk in the American Southwest and Central Plains, *Sci. Adv.*, *1*(1), e1400082, doi:10.1126/sciadv.1400082.

Dai, A. (2011), Characteristics and trends in various forms of the Palmer Drought Severity Index during 1900–2008, *J. Geophys. Res.*, *116*(12), D12115, doi:10.1029/2010JD015541.

Dai, A. (2012), Increasing drought under global warming in observations and models, *Nat. Clim. Change*, *3*(1), 52–58, doi:10.1038/nclimate1633.

Dirmeyer, P. A., G. Fang, Z. Wang, P. Yadav, and A. Milton (2014), Climate change and sectors of the surface water cycle in CMIP5 projections, *Hydrol. Earth Syst. Sci.*, *18*(12), 5317–5329, doi:10.5194/hess-18-5317-2014.

Dominguez, F., P. Kumar, and E. R. Vivoni (2008), Precipitation recycling variability and ecoclimatological stability—a study using NARR data. Part II: North American monsoon region, *J. Clim.*, *21*(20), 5187–5203, doi:10.1175/2008jcli1760.1.

Greve, P., and S. I. Seneviratne (2015), Assessment of future changes in water availability and aridity, *Geophys. Res. Lett.*, *5*, 1–7, doi:10.1002/2015GL064127.

Greve, P., B. Orlowsky, B. Mueller, J. Sheffield, M. Reichstein, and S. I. Seneviratne (2014), Global assessment of trends in wetting and drying over land, *Nat. Geosci.*, *7*(10), 716–721, doi:10.1038/ngeo2247.

Held, I. M., and B. J. Soden (2006), Robust responses of the hydrological cycle to global warming, *J. Clim.*, *19*(21), 5686–5699, doi:10.1175/jcli3990.1.
Huang, J. C., S. J. Kao, M. L. Hsu, and J. C. Lin (2006), Stochastic procedure to extract and to integrate landslide susceptibility maps: an example of mountainous watershed in Taiwan, *Nat. Hazards Earth Syst. Sci.*, *6*, 803–815, doi:10.5194/nhess-6-803-2006.
Huang, J.-C., T.-Y. Lee, and J.-Y. Lee (2014), Observed magnified runoff response to rainfall intensification under global warming, *Environ. Res. Lett.*, *9*(3), 034008–034008, doi:10.1088/1748-9326/9/3/034008.
Intergovernmental Panel on Climate Change (2012), *Managing the Risks of Extreme Events and Disasters to Advance Climate Change Adaptation. A Special Report of Working Groups I and II of the Intergovernmental Panel on Climate Change*, pp. 582, Cambridge Univ. Press, Cambridge, UK and New York.
Kumagai, T. o., G. G. Katul, A. Porporato, T. M. Saitoh, M. Ohashi, T. Ichie, and M. Suzuki (2004), Carbon and water cycling in a Bornean tropical rainforest under current and future climate scenarios, *Adv. Water Resour.*, *27*(12), 1135–1150, doi:10.1016/j.advwatres.2004.10.002.
Kumar, S., D. M. Lawrence, P. A. Dirmeyer, and J. Sheffield (2014), Less reliable water availability in the 21st century climate projections, *Earth's Future*, *2*, 152–160, doi:10.1002/2013EF000159.
Kumar, S., R. Allan, F. Zwiers, D. M. Lawrence, and P. A. Dirmeyer (2015), Revisiting trends in wetness and dryness in the presence of internal climate variability and water limitations over land, *Geophys. Res. Lett.*, *42*, 10867–10875, doi:10.1002/2015GL066858.
Landerer, F. W., and S. C. Swenson (2012), Accuracy of scaled GRACE terrestrial water storage estimates, *Water Resour. Res.*, *48*(4), 1–11, doi:10.1029/2011WR011453.
Lawrence, D., and K. Vandecar (2015), Effects of tropical deforestation on climate and agriculture, *Nat. Clim. Change*, *5*(1), 27–36, doi:10.1038/nclimate2430.
Liu, S. C., C. B. Fu, C. J. Shiu, J. P. Chen, and F. T. Wu (2009), Temperature dependence of global precipitation extremes, *Geophys. Res. Lett.*, *36*(17), 1–4, doi:10.1029/2009GL040218.
Lo, M. H., P. J. F. Yeh, and J. S. Famiglietti (2008), Constraining water table depth simulations in a land surface model using estimated baseflow, *Adv. Water Resour.*, *31*(12), 1552–1564, doi:10.1016/j.advwatres.2008.06.007.
Malhi, Y., and J. Grace (2000), Tropical forests and atmospheric carbon dioxide, *Trends Ecol. Evol.*, *15*, 332–337, doi:10.1016/s0169-5347(00)01906-6.
Malhi, Y., C. Doughty, and D. Galbraith (2011), The allocation of ecosystem net primary productivity in tropical forests, *Philos. Trans. R. Soc. B*, *366*(1582), 3225–3245, doi:10.1098/rstb.2011.0062.
Malhi, Y., S. Adu-Bredu, R. A. Asare, S. L. Lewis, and P. Mayaux (2013), African rainforests: past, present and future, *Philos. Trans. R. Soc. B*, *368*(1625), 20120312, doi:10.1098/rstb.2012.0312.
Mathison, C., a. J. Wiltshire, P. Falloon, and a. J. Challinor (2015), South Asia river flow projections and their implications for water resources, *Hydrol. Earth Syst. Sci. Discuss.*, *12*(6), 5789–5840, doi:10.5194/hessd-12-5789-2015.
Nearing, M. A., F. F. Pruski, and M. R. O'Neal (2004), Expected climate change impacts on soil erosion rates: a review, *J. Soil Water Conserv.*, *59*, 43–50.
O'Gorman, P. A., and T. Schneider (2009), The physical basis for increases in precipitation extremes in simulations of 21st-century climate change, *Proc. Natl. Acad. Sci. U. S. A.*, *106*(35), 14773–14777, doi:10.1073/pnas.0907610106.
Oki, T., and Y. C. Sud (1998), Design of Total Runoff Integrating Pathways (TRIP)—a global river channel network, *Earth Interact.*, *2*(1), 1, doi:10.1175/1087-3562(1998)002<0001:DOTRIP>2.3.CO;2.
Phillips, O. L., S. L. Lewis, T. R. Baker, and Y. Malhi (2007), The response of South American tropical forests to contemporary atmospheric change, in *Tropical Rainforest Responses to Climatic Change*, edited by M. B. Bush and J. R. Flenley , pp. 317–332 , Springer-Praxis Publ. Ltd., New York.
Reynolds, G., J. Payne, W. Sinun, G. Mosigil, and R. P. Walsh (2011), Changes in forest land use and management in Sabah, Malaysian Borneo, 1990–2010, with a focus on the Danum Valley region, *Philos. Trans. R. Soc. B*, *366*(1582), 3168–3176, doi:10.1098/rstb.2011.0154.
Rudolf, B., A. Becker, U. Schneider, A. Meyer-Christoffer, and M. Ziese (2010). GPCC Status Report December 2010, On the most recent gridded global data set issued in fall 2010 by the Global Precipitation Climatology Centre (GPCC). [Available at http://gpcc.dwd.de]
Santer, B. D., et al. (2007), Identification of human-induced changes in atmospheric moisture content, *Proc. Natl. Acad. Sci. U. S. A.*, *104*(39), 15248–15253, doi:10.1073/pnas.0702872104.
Seager, R., N. Naik, and G. A. Vecchi (2010), Thermodynamic and dynamic mechanisms for large-scale changes in the hydrological cycle in response to global warming, *J. Clim.*, *23*(17), 4651–4668, doi:10.1175/2010jcli3655.1.
Sheffield, J., E. F. Wood, and M. L. Roderick (2012), Little change in global drought over the past 60 years, *Nature*, *491*(7424), 435–438, doi:10.1038/nature11575.
Sheffield, J., et al. (2013), North American climate in CMIP5 experiments. Part I: Evaluation of historical simulations of continental and regional climatology, *J. Clim.*, *26*(23), 9209–9245, doi:10.1175/jcli-d-12-00592.1.
Sun, Y., S. Solomon, A. Dai, and R. W. Portmann (2007), How often will it rain? *J. Clim.*, *20*(19), 4801–4818, doi:10.1175/jcli4263.1.
Tan, J., C. Jakob, W. B. Rossow, and G. Tselioudis (2015), Increases in tropical rainfall driven by changes in frequency of organized deep convection, *Nature*, *519*(7544), 451–454, doi:10.1038/nature14339.
Tan, P. H., C. Chou, and J. Y. Tu (2008), Mechanisms of global warming impacts on robustness of tropical precipitation asymmetry, *J. Clim.*, *21*, 5585–5602, doi:10.1175/2008jcli2154.1.
Tapley, B. D., S. Bettadpur, M. Watkins, and C. Reigber (2004), The gravity recovery and climate experiment: mission overview and early results, *Geophys. Res. Lett.*, *31*(9), 1–4, doi:10.1029/2004GL019920.
Taylor, K. E., R. J. Stouffer, and G. A. Meehl (2012), An overview of CMIP5 and the experiment design, *Bull. Am. Meteorol. Soc.*, *93*(4), 485–498, doi:10.1175/bams-d-11-00094.1.
Trenberth, K. E., A. Dai, R. M. Rasmussen, and D. B. Parsons (2003), The changing character of precipitation, *Bull. Am. Meteorol. Soc.*, *84*(9), 1205–1217, doi:10.1175/bams-84-9-1205.
Vecchi, G. A., and B. J. Soden (2007), Global warming and the weakening of the tropical circulation, *J. Clim.*, *20*(17), 4316–4340, doi:10.1175/jcli4258.1.
Wu, W.-Y., C.-W. Lan, M.-H. Lo, J. T. Reager, and J. S. Famiglietti (2015), Increases in the annual range of soil water storage at northern middle and high latitudes under global warming, *Geophys. Res. Lett.*, *42*(10), 3903–3910, doi:10.1002/2015GL064110.
Zhang, X., F. W. Zwiers, G. C. Hegerl, F. H. Lambert, N. P. Gillett, S. Solomon, P. A. Stott, and T. Nozawa (2007), Detection of human influence on twentieth-century precipitation trends, *Nature*, *448*(7152), 461–465, doi:10.1038/nature06025.

Zhang, X., L. Alexander, G. C. Hegerl, P. Jones, A. K. Tank, T. C. Peterson, B. Trewin, and F. W. Zwiers (2011), Indices for monitoring changes in extremes based on daily temperature and precipitation data, *WIREs Clim. Change*, *2*, 851–870, doi:10.1002/wcc.147.

Zhang, X., Q. Tang, X. Zhang, and D. P. Lettenmaier (2014), Runoff sensitivity to global mean temperature change in the CMIP5 Models, *Geophys. Res. Lett.*, *41*, 5492–5498, doi:10.1002/2014GL060382.

Zhao, T., and A. Dai (2015), The magnitude and causes of global drought changes in the twenty-first century under a low–moderate emissions scenario, *J. Clim.*, *28*(11), 4490–4512, doi:10.1175/jcli-d-14-00363.1.